mathematics

MDPI

Article

Development and Application of a Multi-Objective Tool for Thermal Design of Heat Exchangers Using Neural Networks

José Luis de Andrés Honrubia [1], José Gaviria de la Puerta [1], Fernando Cortés [1], Urko Aguirre-Larracoechea [2], Aitor Goti [1,*] and Jone Retolaza [3]

[1] Deusto Digital Industry Chair, Faculty of Engineering, University of Deusto, Avda. Universidades 24, 48080 Bilbao, Spain; jlandresh@opendeusto.es (J.L.d.A.H.); jgaviria@deusto.es (J.G.d.l.P.); fernando.cortes@deusto.es (F.C.)
[2] Faculty of Health Sciences, University of Deusto, Avda. Universidades 24, 48080 Bilbao, Spain; u.agirre@deusto.es
[3] Accenture Bilbao Industry X.0 Center, Parque Tecnológico de Bizkaia, Astondo Bidea, Edificio 602, 48160 Bilbao, Spain; jone.retolaza@accenture.com
* Correspondence: aitor.goti@deusto.es

Abstract: This paper presents the design of a multi-objective tool for sizing shell and tube heat exchangers (STHX), developed under a University/Industry collaboration. This work aims to show the feasibility of implementing artificial intelligence tools during the design of Heat Exchangers in industry. The design of STHX optimisation tools using artificial intelligence algorithms is a visited topic in the literature, nevertheless, the degree of implementation of this concept is uncommon in industrial companies. Thus, the challenge of this research consists of the development of a tool for the design of STHX using artificial intelligence algorithms that can be used by industrial companies. The approach is implemented using a simulated dataset contrasted with ARA TT, the company taking part in the project. The given dataset to develop a theoretical STHX calculator was modeled using MATLAB. This dataset was used to train seven neural networks (NNs). Three of them were mono-objective, one per objective to predict, and four were multi-objective. The last multi-objective NN was used to develop an inverse neural network (INN), which is used to find the optimal configuration of the STHXs. In this specific case, three design parameters, the pressure drop on the shell side, the pressure drop on the tube side and heat transfer rate, were jointly and successfully optimised. As a conclusion, this work proves that the developed tool is valid in both terms of effectiveness and user-friendliness for companies like ARA TT to improve their business activity.

Keywords: shell and tube heat exchangers; neural networks; multi-objective optimisation; industrial application

check for updates

Citation: de Andrés Honrubia, J.L.; de la Puerta, J.G.; Cortés, F.; Aguirre-Larracoechea, U.; Goti, A.; Retolaza, J. Development and Application of a Multi-Objective Tool for Thermal Design of Heat Exchangers Using Neural Networks. *Mathematics* **2021**, *9*, 1120. https://doi.org/10.3390/math9101120

Academic Editors: Mikhail Zymbler and Sachin Kumar

Received: 26 March 2021
Accepted: 12 May 2021
Published: 15 May 2021

Publisher's Note: MDPI stays neutral with regard to jurisdictional claims in published maps and institutional affiliations.

Copyright: © 2021 by the authors. Licensee MDPI, Basel, Switzerland. This article is an open access article distributed under the terms and conditions of the Creative Commons Attribution (CC BY) license (https://creativecommons.org/licenses/by/4.0/).

1. Introduction

Heat transfer applications have been studied over the last decades. This analysis has ranged from more traditional and simple forms [1], to much more complex ones [2]. Despite its long history, it remains as an interesting research area with a long way to investigate [3]. From a more industrial view, heat transfer is the basic phenomenon behind the heat exchangers, which are widely used industrial equipment in many sectors.

Heat exchangers are used in multiple scopes, for this reason, there are a lot of different types of configurations. Two of the most common and important models are shell and tube heat exchangers (STHX) and plate-fin heat exchangers (PFHX). Both are widely used in countless industries, such as process, power, transportation, air-conditioning and refrigeration, heat recovery, alternate fuels, and manufacturing industry. These heat exchangers are, as well, key components of numerous industrial products available in the marketplace. STHX are more commonly found in process industries, in conventional and nuclear power stations as condensers, in pressurised and water reactor plants as steam

generators, as feedwater heaters, etc. On the other hand, PFHX are typical compact heat exchangers which are found to have several applications in the industries of petroleum, petrochemical, chemical and power generation [4–8]. Figure 1 shows one of the simplest configurations of a STHX. This is a one-shell and two-pass through the tube's configuration, also referred to as STHX (1-2).

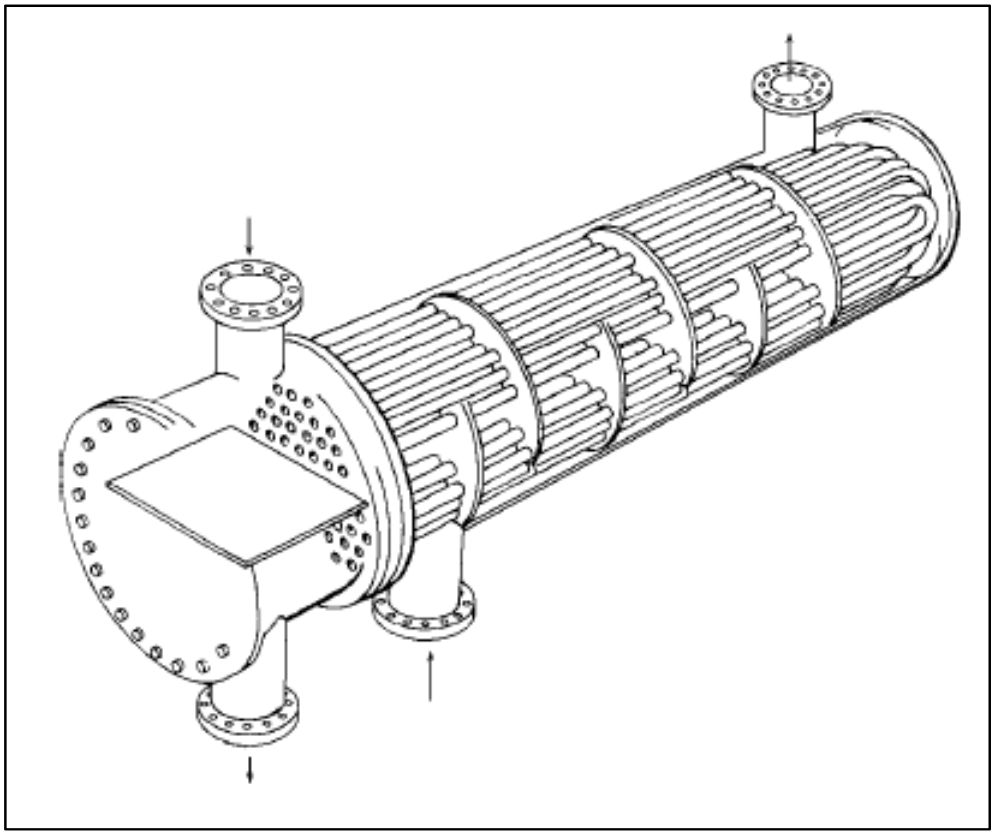

Figure 1. STHX (1-2) [9].

There are numerous types of heat exchangers which have been investigated in a variety of ways through the last decades. Since the beginning of this century, heat exchangers have been explored in countless publications. In Dezfoli et al. [10], plate heat exchangers were studied. In this study, analytical solutions are developed to solve the two-dimensional (2D) temperature changes of flow in the passages of a plate heat exchanger in parallel flow and counter flow arrangements. Other types of as compact heat exchangers (CHX), helical coil heat exchangers (HCHX) or STHX were also studied. In [11] the enhancement effect of suspended graphene nano-platelets in coolant fluids used in CHX was proved. Lazova et al. [12] showed that for a better estimation of the HCHX size, a more accurate correlation is required to design an optimal configuration and thus employ cheaper components. Lastly in Yang et al. [13] four different STHX modeling approaches were developed and validated with experimental results.

In conclusion, given the previous conditions, the aim of this work is to demonstrate that it is possible to develop a practical tool for the company ARA TT to size STHX from a multi-objective optimisation perspective, using artificial intelligence techniques, specifically neural networks (NNs). Thus, the presented study is structured as follows: Section 2 presents the related work, briefly describes what a NN is and summarises the main findings of the paper. Section 3 details both (i) the mathematical model of the STHX to generate the dataset used to train the developed NN optimisation tool and (ii) the optimisation tool itself. Section 4 describes how the NN model was trained and validated. Then, Section 5 explains the problem formulation and optimisation procedure of the actual application case shown afterwards in Section 6, where the results of the application are

as well illustrated. Finally, Section 7 includes the discussion and limitations of the study, while Section 8 presents the concluding remarks, pinpointing that the obtained results raised the interest of the other industrial partners.

2. Related Work

For a long time, the use of computational analysis has been becoming a popular and indispensable research field. For example, in 2003, Sahoo et al. [14] developed a computer based iterative solution for helical tube exchangers. However, it is now common knowledge that technology is incredibly growing in potential, and this is not an exception in the field. In Sun et al. [15] more up-to-date software solutions were already used. In this study, a combination between computer fluids dynamics (CFD) software and a genetic algorithm were used to determine the optimal solution for a STHX with inclined trefoil-hole baffles.

Artificial intelligence algorithms are getting more and more popular. Lots of papers are including this type of analysis in their studies. As indicated in Rao et al. [5], "In recent years the application of advanced optimisation algorithms for design problems of heat exchangers has gained much momentum." This paper incorporates a considerable resume about some existent methods: the genetic algorithm (GA), used in several investigation papers of different topics [16,17]; the artificial bee colony (ABC) algorithm; the particle swarm optimisation (PSO), explained in [18]; or the simulated annealing (SA) algorithm, which is used occasionally with other algorithms, like in Su et al. [19] where it is combined with PSO algorithm. These and some variants of them are among the most used algorithms.

To harness the power of computational analysis, heat exchanger studies are increasingly focused on obtaining multi-objective solutions. Typically, the procedure is achieved by using an evolutionary algorithm to model the study case. However, there are several types of genetic algorithms. One of the most popular is the self-organising-map (SOM), which was used, for example, in Tan et al. [20] to model the performance of a compact heat exchanger. Regarding multi-objective evolutionary algorithms (MOEAs), the two that are probably the most common are the multi-objectives genetic algorithm (MOGA), used in Wen et al. [21], and the non-dominated sorting genetic algorithm-II (NSGA-II) which is very much seen in more industrial terms [15,22,23]. Additionally, in the last years, solutions combining MOEAs for a fast convergence in the optimisation process with NNs have been developed [24,25].

Artificial neural networks (ANNs) or NNs are mathematical models based on the animals' nervous systems. Recently, they have been successfully applied around data mining, due to their ability to generate models effectively and efficiently, as well as to search for patterns in the data.

These networks are composed of a group of interconnected artificial neurons. In most cases, such networks are an adaptive system that changes its structure depending on the information flowing through the network in the learning phase.

Although there is no precise definition all researchers agree on, it is known to be a network of simple processing elements (neurons), which can exhibit complex overall behaviour, determined by the connections between the elements of the process and by the parameters of those elements.

In recent years, the use of NNs has grown exponentially. The different models that exist have been used in different areas. RBF (radial basis function) networks, Hopfield networks or stochastic NNs are some of the most widely used types. On the other hand, the combination of these types of networks by means of genetic algorithms is becoming more and more frequent. Thus, the evolution of NNs in the coming years looks promising.

The literature shows that optimising heat exchanger size and work parameters (like pressure drop, heat transfer rate, geometrical parameters, etc.) along with total cost, is very important condition for the efficiency and the optimisation concept has been investigated for several years [26–28]. Nevertheless, the number of industrial companies using artificial intelligence optimisation tools in this field seems to be scarce. As in other areas such as logistics, the reason behind this lack of implementation can be inefficient collaboration

between researchers and companies. Even though researchers develop solutions to the problem, they are mainly focused on publishing and not on developing final products to be used by companies [29].

In this specific case of optimisation of STHXs, the use of certain tools proposed in the literature can have limited applicability in companies, as they tend to have turnkey solutions that are reliable and easy to maintain. GAs have problems to deal with complexity and scalability of the problem to be optimised [30]. Nevertheless, these changes in complexity and scalability are common in industries; each customer can impose additional restrictions (e.g., geometrical ones, regulatory aspects), and as a consequence changing the equation models needed for the STHX optimisation tool. Similarly, it can be said that solutions to the STHX case using tools such as the aforementioned PSO, SA, ABC, are valid now of their implementation, but if the model must scale, they need further developments, so they cannot be used as a stand-alone solution for a company.

Due to these simplicity and adaptability needs and scarcity of the publications about the implementation multi-objective NNs in the literature, research team decided to implement this technique as stand-alone solution for the company involved in this research. Therefore, one of the contributions of this work is the development of a tool that is accurately applicable to a real industrial environment.

A relevant novelty of this research is as well the use of an inverse neural network (INN) for the finding the optimal solutions, as this has never been done in the case of STHX. NNs are not capable of offering by themselves optimal or suboptimal configurations for an optimisation problem. To make the NN capable of offering STHX configuration solutions fitting the specified requirements imposed to a problem, an INN has been coupled to the NN. This INN is used to find all the valid configuration solutions of the STHXs that are afterwards filtered and selected implementing a Pareto front approach.

Another innovative fact of this research is the algorithm used in the NNs, as it has not been used for this type of application case before. This NNs uses the RELU [31] algorithm, and serves as the artificial intelligence model to obtain the outputs of the heat exchangers. This NNs uses as loss function the meaan square error algorithm and as metric validation the mean absolute error, this metric is used in the literature for algorithm validation as can be seen in the paper by Chai and Draxler [32]. This would give us a huge amount of valid STHX, that is why a multi-objective NN is implemented to find the optimum STHX for some specifications given [33].

3. Materials and Methods

In this study heat exchangers from ARA TT [34] were analysed, which are STHX with segmental baffles. Based on these heat exchangers, a simulated dataset was generated. It was based on the ARA's catalogue, the Tubular Exchanger Manufacturers Association (TEMA) standards and the principles of heat transfer. This dataset was used to train seven NNs specifically created to size heat exchangers applying mono- and multi-objective optimisation.

The purpose of the STHX studied in this work is to cool the lubricating oil involved in an industrial process. There are 11 design variables. Seven of them are from the STHX design: the shell inner diameter, the number of tubes, the number of steps per tube, the tube outer diameter (that has associated a specific tube thickness), the tube length, the tube pitch, and the baffles separation. The other four ones are related to the fluids: oil mass flow, oil entry temperature, water mass flow and water entry temperature.

This work pretended to optimise the selection of the 11 design variables abovementioned due to their effect in the heat rate, the pressure drop in the shell side and the pressure drop in the tube side. To achieve this, the first step was to generate a synthetic dataset starting from an existing STHX provided by the collaborator company ARA TT. Tables 1–4 show the information about the data used in this work. The data could be of three different types:

1. The variable data are the ones that its value is changing for each case to get the database, which corresponds also with the 11 (aforementioned) design parameters.
2. The static simulation data, which take a static value in each simulation case, but its value depends on something like temperature or material type.
3. The output variables, which are the results of final and intermediate calculations.

Additionally, in Tables 1–3 the column "reference value" is presented, which corresponds to the heat exchanger case validated by ARA TT.

Oil and water properties are dependent on temperature. In the following equations of Section 3.1, the properties values at the average temperature will be used. The specific values of the static variables were provided by ARA TT [35].

The inner diameter depends on the selected tube. Each type of tube has an outer diameter associated to a specific thickness that allows to get the tube inner diameter d_{inn}.

Table 1. General heat exchanger parameters.

Equipment Data	Abbreviation	Reference Value	Unit	Type
Shell inner diameter	d_{ic}	432	[mm]	Variable
Number of tubes	N	173	[units]	Variable
Number of steps per tube	n	2	[units]	Variable
Tube outer diameter	d_{out}	16	[mm]	Variable
Tube inner diameter	d_{inn}	Depends on tube outer diameter	[mm]	Static
Tube thickness	e	1.5	[mm]	Static
Tube length (for step)	L	2050	[mm]	Variable
Tube conductivity	k	14.02	[kcal(h m °C)]	Static
Tube pitch	P	20	[mm]	Variable
Baffle's thickness	e_{baffles}	4.8	[mm]	Static
Baffle's separation	BS	200	[mm]	Variable
Inner fouling resistance	${h_{\text{foul}_{\text{inn}}}}^{-1}$	0.00023	$\left[\left(\text{hm}^2\ ^\circ\text{C}\right)\text{kcal}\right]$	Static
Outer fouling resistance	${h_{\text{foul}_{\text{out}}}}^{-1}$	0.00023	$\left[\left(\text{hm}^2\ ^\circ\text{C}\right)\text{kcal}\right]$	Static

Table 2. Oil variables.

Oil Variables	Abbreviation	Reference Value	Unit	Type
Mass flow	$\dot{m}_{\text{oil}}$	51900	[kgh]	Variable
Entry temperature	T_1	40	[°C]	Variable
Exit temperature	T_2	-	[°C]	Output
Average temperature	T_{m}	-	[°C]	Output
Density	ρ_{oil}	Dependent on temperature	$[\text{kgm}^3]$	Static
Dynamic viscosity	μ_{oil}	Dependent on temperature	[Pa s]	Static
Kinematic viscosity	ν_{oil}	Dependent on temperature	$[\text{m}^2\text{s}]$	Static
Thermal conductivity	k_{oil}	Dependent on temperature	[kcal(hm °C)]	Static
Specific heat capacity	cp_{oil}	Dependent on temperature	[kcalkg °C]	Static
Prandtl number	Pr_{oil}	107.5	-	Static

Table 3. Water variables.

Water Variables	Abbreviation	Reference Value	Unit	Type
Mass flow	$\dot{m}_{\mathrm{w}}$	30000	[kgh]	Variable
Entry temperature	t_1	25	[°C]	Variable
Exit temperature	t_2	-	[°C]	Output
Average temperature	t_{m}	-	[°C]	Output
Density	ρ_{w}	Dependent on temperature	$[\mathrm{kgm}^3]$	Static
Dynamic viscosity	μ_{w}	Dependent on temperature	[Pa s]	Static
Kinematic viscosity	ν_{w}	Dependent on temperature	$[\mathrm{m}^2\mathrm{s}]$	Static
Thermal conductivity	k_{w}	Dependent on temperature	[kcalhm °C]	Static
Specific heat capacity	cp_{w}	Dependent on temperature	[kcalkg °C]	Static

Table 4. Heat exchanger results.

Results Variables	Abbreviation	Unit	Type
Heat exchanged	$\dot{Q}$	[kcalh]	Output
Pressure drop on shell side	hL_{shell}	[bar]	Output
Pressure drop on tube side	hL_{tube}	[bar]	Output

3.1. Heat Exchanger Model

3.1.1. Exchanged Heat

As previously mentioned, the solving method is a process based on several iterations to create a dataset for training the NNs. The variable for generating the iterations is the oil exit temperature T_2 starting in every stage from $T_2 = 34.10$ °C.

To generate the whole dataset, the data (of variable type according to Tables 1–3) consisted of three different values. The first one corresponds to the reference value column presented in Tables 1–3. The next two cases are the 85% and the 115% of this reference value. The only exception is the number of steps which the values one, two and three steps took. As there are 11 design variables that vary between three different values, a dataset was generated with 3^{11} cases (177.147 dissimilar heat exchangers instances).

The solution method developed in this paper allows to obtain all the numerical outputs associated to each instance of the dataset. This is done by iterating with the oil exit temperature T_2 checking if the exchanged heat $\dot{Q}$ obtained with Equations (1) and (2) match. The process continues checking results until both match and each value is fixed. It is at this point that the outputs are recorded as an instance of the dataset.

The exchanged heat $\dot{Q}$ between both fluids is obtained from the enthalpy balance, given by

$$\dot{Q} = \dot{m}_{\mathrm{oil}}\, cp_{\mathrm{oil}}\, \Delta T = \dot{m}_{\mathrm{w}}\, cp_{\mathrm{w}}\, \Delta t\,, \tag{1}$$

where ΔT represents the oil temperature difference and Δt the water temperature difference; it means that $\Delta T = T_2 - T_1$ and $\Delta t = t_2 - t_1$. At the same time, $\dot{Q}$ depends on the heat exchanger parameters, specifically, the *LMTD* method states that [36]

$$\dot{Q} = U{\cdot}A{\cdot}F{\cdot}LMTD. \tag{2}$$

In Equation (2) U indicates the overall heat exchanger coefficient, the A refers to the equipment exchange area, the *LMTD* represents the logarithmic mean temperature difference for double tube heat exchanger in counterflow and the F factor is the *LMTD*

correction factor that takes into account configurations different to the double tube one. The calculations for each of the terms are detailed below.

First of all, the *LMTD* results in

$$LMTD = \frac{(T_1 - t_2) - (T_2 - t_1)}{\ln \frac{T_1 - t_2}{T_2 - t_1}} \, . \tag{3}$$

The exchange surface A is given by

$$A = \pi \, d_{\text{out}} \, L \, n \, N - A_{\text{baffles}} \, , \tag{4}$$

where the whole tube outer surface minus the area occupied by the baffles is considered. This area A_{baffles} is estimated by

$$A_{\text{baffles}} = n_{\text{baffles}} \, \pi \, n \, X_{\text{baffles}} \, e_{\text{baffle}} \, . \tag{5}$$

To determine the space occupied by the baffles, which is not useful for the heat exchange, some new parameters as shown in Equation (5) are needed. The first one is the number of baffles, which are calculated with

$$n_{\text{baffles}} = \frac{L}{BS} \, , \tag{6}$$

and the second one is the percentage of tubes affected by baffles. To estimate this value, the free space on the shell side left by the baffle is needed, which is obtained through the diameter percentage of free space in each baffle section $FD_{\text{percentage}}$. In this case, the numeric value of the $FD_{\text{percentage}}$ is provided by the company ARA TT and it corresponds to the 26% of the inner shell diameter d_{ic}. All this results in

$$X_{\text{baffles}} = 1 - \frac{\theta - \sin \theta}{2 \, \pi} \, , \tag{7}$$

where

$$\theta = 2 \, \cos^{-1}\left(1 - 2 \, FD_{\text{percentage}}\right) \, . \tag{8}$$

The correction factor F is a correction to the *LMTD* that takes into account that the equipment studied is not the double tube and one step heat exchanger.

For this reason, when the analysed exchanger is a STHX with multiple tubes, this correction must be applied.

For the cases in which it is necessary to apply this F factor, its numerical value depends on the number of steps the heat exchanger has. When it has one step, this factor is almost one, if the distances between the deflectors are those established in the TEMA Standard. For the case of two tube steps, F can be obtained by (as explained in [9])

$$F = \frac{\left(\frac{\sqrt{(T_1 - T_2)^2 + (t_2 - t_1)^2}}{\ln\left(\frac{(T_1 + T_2) - (t_1 + t_2) + \sqrt{(T_1 - T_2)^2 + (t_2 - t_1)^2}}{(T_1 + T_2) - (t_1 + t_2) - \sqrt{(T_1 - T_2)^2 + (t_2 - t_1)^2}} \right)} \right)}{LMTD} \, . \tag{9}$$

For the case of three tube steps an analytical equation does not exist. Thus, for that case, the F factor could be obtained with Figure 2.

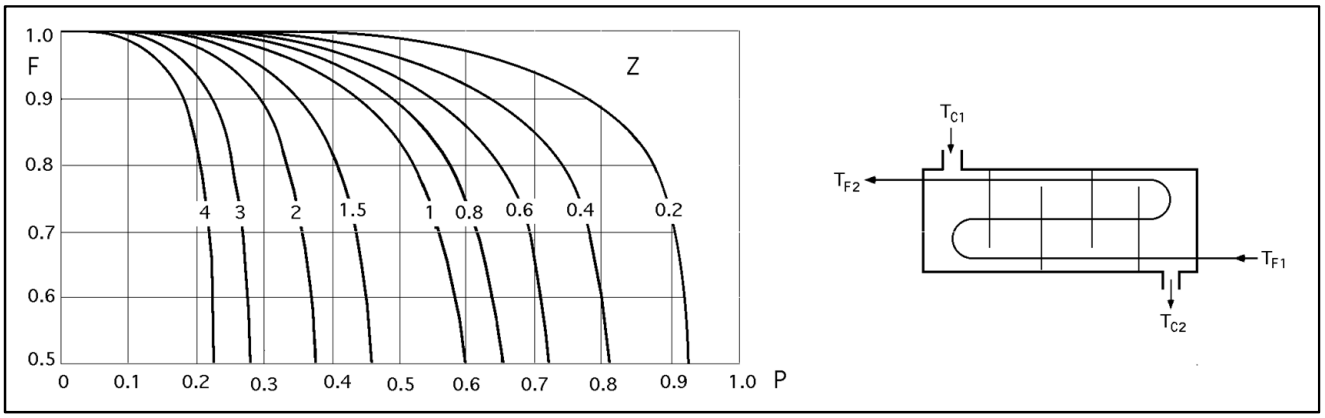

Figure 2. Correction factor F, for heat exchanger with one shell step and three tube steps [9].

Finally, the overall heat transfer coefficient is given by [37]

$$UA = \frac{1}{R_s} = \frac{1}{R_{\text{foul}_{\text{inn}}} + R_{\text{foul}_{\text{out}}} + R_{\text{cond}} + R_{\text{conv}_{\text{inn}}} + R_{\text{conv}_{\text{out}}}}. \tag{10}$$

This overall heat transfer coefficient is defined by the total thermal conductance given by the inner and outer convection thermal resistance ($R_{\text{conv}_{\text{out}}}$, $R_{\text{conv}_{\text{inn}}}$), the tube conduction thermal resistance R_{cond} and the inner and outer fouling thermal resistance ($R_{\text{foul}_{\text{out}}}$, $R_{\text{foul}_{\text{inn}}}$). This equation derives in (see for example [37,38] for the details)

$$U = \frac{1}{{h_{\text{foul}_{\text{inn}}}}^{-1} \frac{d_{\text{out}}}{d_{\text{inn}}} + {h_{\text{foul}_{\text{out}}}}^{-1} + \ln\left(\frac{d_{\text{out}}}{d_{\text{inn}}}\right) \frac{d_{\text{out}}}{2k} + \frac{1}{h_{\text{inn}}} \frac{d_{\text{out}}}{d_{\text{inn}}} + \frac{1}{h_{\text{out}}}}. \tag{11}$$

where h_{inn} and h_{out} are the convection heat transfer coefficients for the inner and the outer sides, respectively.

For the convection heat transfer coefficient in the inner side is required to get some new parameters. These convection coefficients are obtained from pseudo-empirical correlations, starting from

$$h_{\text{inn}} = Nu_{\text{w}} \frac{k_{\text{w}Tm}}{d_{\text{inn}}}, \tag{12}$$

where the Nusselt number Nu is a dimensionless number that represents the ratio of convective to conductive heat transfer at a boundary layer. Nu is obtained with Equations (13) and (14) for laminar flow and turbulent flow, respectively, as explained in [39].

The expression for laminar flow results in

$$Nu_{\text{w}} = 1.86 \, (Re_{\text{w}} \, Pr_{\text{w}})^{\frac{1}{3}} \left(\frac{d_{\text{inn}}}{L}\right)^{\frac{1}{3}} \left(\frac{\mu}{\mu_p}\right)^{0.14}, \tag{13}$$

where the term $\left(\frac{d_{\text{inn}}}{L}\right)^{\frac{1}{3}}$ is a correction factor that only applies if the tube is not long enough for the laminar flow to fully develop and $\left(\frac{\mu}{\mu_{\text{p}}}\right)^{0.14}$ is another correction factor that is only used if there is a considerable temperature gradient between the tube wall and the boundary layer.

On the other side, the expression for turbulent flow is

$$Nu_{\text{w}} = 0.023 \, {Re_{\text{w}}}^{0.8} \, {Pr_{\text{w}}}^{n} \tag{14}$$

where n value is 0.4 because the fluid is receiving heat (otherwise, n would be 0.3).

Reynolds number Re is a dimensionless number and expresses the ratio between inertial forces and viscous forces within a fluid that is subjected to relative internal movement due to different fluid velocities.

Laminar flow means that Reynolds number Re is less than 2000 and for turbulent flow the value is higher than 10,000. Laminar flow is characterised by smooth, constant fluid motion, while turbulent flow tends to produce chaotic eddies, vortices and other flow instabilities.

The expression to get Reynolds number is

$$Re_{\mathrm{w}} = \frac{vel_{\mathrm{tube}}\, \rho_{\mathrm{w}}\, d_{\mathrm{inn}}}{\mu_{\mathrm{w}}} \ , \tag{15}$$

where the term vel_{tube} refers to the fluid velocity inside the tubes. This is derived from the water mass flow $\dot{m}_{\mathrm{w}}$, the water density ρ_{w} and the tube flow cross sectional area as A_{tube}

$$vel_{\mathrm{tube}} = \frac{\dot{m}_{\mathrm{w\,tube}}}{\rho_{\mathrm{w}}\, A_{\mathrm{tube}}} \ . \tag{16}$$

The other part needed to calculate Nu is the Prandtl number Pr, given by

$$Pr_{\mathrm{w}} = \frac{\nu_{\mathrm{w}}}{\alpha_{\mathrm{w}}} \ , \tag{17}$$

where the water thermal diffusivity α_{w} depends on temperature and results from

$$\alpha_{\mathrm{w}} = \frac{k_{\mathrm{w}}}{\rho_{\mathrm{w}}\, cp_{\mathrm{w}}} \ . \tag{18}$$

The convection heat transfer coefficient in the outer side h_{ext} is given by

$$h_{\mathrm{ext}} = Nu_{\mathrm{oil}}\, \frac{k_{\mathrm{oil}_{Tm}}}{d_{\mathrm{e}}} \ . \tag{19}$$

To get the value of Nu_{oil} the expressions shown in Equations (13) and (14) adapted to the outer side are used. All the variables need to be referred to the outer fluid (oil) and to the outer side of tubes. In this case the exponent n in Equation (14) value is 0.3 because it is referring to the hotter fluid, which yields heat to the cooler fluid.

Returning to the convection heat transfer coefficient in the outer side, the hydraulic diameter d_{e} is used. This hydraulic diameter is defined by

$$d_{\mathrm{e}} = \frac{4\, A_{\mathrm{long}}}{Pe_{\mathrm{wetted}}} \ , \tag{20}$$

where the cross-sectional area A_{long} and the wetted perimeter Pe_{wetted} depend on the tube configuration. For the staggered layout used in this paper, the expressions for these terms are

$$Pe_{\mathrm{wetted}} = \frac{\pi\, d_{\mathrm{out}}}{2} \ , \tag{21}$$

and

$$A_{\mathrm{long}} = \frac{P^2\, \sqrt{2}}{4} - \frac{\pi\, {d_{\mathrm{out}}}^2}{8} \ . \tag{22}$$

Figure 3 represents the used tube's layout, which is a staggered layout.

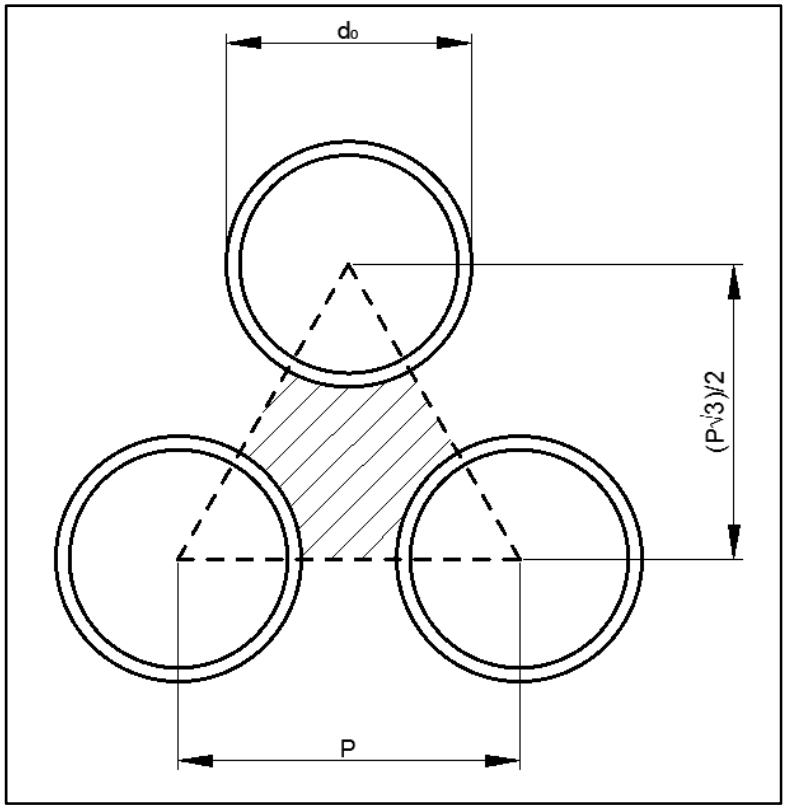

Figure 3. Staggered tubes layout.

For the Reynolds number on the shell side, the calculation of the oil velocity is defined in Equation (23). As this velocity is not uniform due to the baffle's existence, to get it the Donohue method is used. It consists of obtaining the geometric average value of two different velocities as in

$$vel_{\text{shell}} = \sqrt{vel_{\text{shell}_{\text{long}}}\, vel_{\text{shell}_{\text{cross}}}} \quad . \tag{23}$$

The velocity on the shell side is composed with the velocity on two different directions. This is because of the baffles. These velocities are the longitudinal and the transverse velocity.

The first one is given by

$$vel_{\text{shell}_{\text{long}}} = \frac{m_{\text{oil}}}{\rho_{\text{oil}}\, A_{\text{shell}_{\text{long}}}} \quad , \tag{24}$$

where $A_{\text{shell}_{\text{long}}}$ is the longitudinal passing area shown in

$$A_{\text{shell}_{\text{long}}} = \frac{\left[(d_{\text{ic}})^2 - \left(N\, n\, {d_{\text{out}}}^2\right)\right] \pi\, FD_{\text{percentage}}}{4} \quad . \tag{25}$$

The transverse velocity results in

$$vel_{\text{shell}_{\text{cross}}} = \frac{m_{\text{oil}}}{\rho_{\text{oil}}\, A_{\text{shell}_{\text{cross}}}} \quad . \tag{26}$$

For this cross speed, the cross-passing area $A_{\text{shell}_{\text{cross}}}$ is defined as

$$A_{\text{shell}_{\text{cross}}} = BS{\cdot}[d_{\text{ic}} - (N_{\text{t}}\, d_{\text{out}})] \quad , \tag{27}$$

where the term N_t is the number of tubes in the middle section and is calculated with

$$N_t = \frac{d_{ic}}{P} - 1 \ . \tag{28}$$

3.1.2. Pressure Drop

In the most common STHX configurations, such as those analysed in this article, the fluid in the tubes first enters a tank through a coupling. Subsequently, it enters the interior of the tubes and finally exits into another tank, from which it leaves the exchange equipment.

The pressure loss in the tubes is therefore calculated through the sum of all the singular losses that appear in the path of the fluid, as explained in [40]. Therefore, the total pressure losses hL_{tube} in the tubes are the sum of the losses at the inlet to the first tank hL_{iTank1}, plus the losses at the inlet to the tubes hL_{iTubes}, plus the friction losses in the tubes hL_{fr}, plus the losses in the tube's elbows hL_{elb} (in case of more than one tube step), plus the losses at the outlet of the tubes hL_{oTubes} and plus the losses at the outlet of the second tank hL_{oTank2}, as shown in

$$hL_{tube} = hL_{iTank1} + hL_{iTubes} + hL_{fr} + hL_{elb} + hL_{oTubes} + hL_{oTank2} \ . \tag{29}$$

All these singular losses will depend on the installation made and on the geometry of the equipment, as explained in [40].

For the case of the pressure drop on the shell side hL_{shell}, the Donohue method must be used again, just as done previously to obtain the shell fluid velocity in Equation (23). (for details, see [39]).

This method consists of obtaining the pressure losses due to both longitudinal flow hL_{long} and cross flow hL_{cross}. By combining the two of them, the total losses on the shell side are obtained. These total losses are exposed in

$$hL_{shell} = n_{baffles} hL_{long} + (n_{baffles} + 1) hL_{cross} \ , \tag{30}$$

where $n_{baffles}$ is obtained in Equation (6). While longitudinal losses hL_{long} and cross losses hL_{cross} are obtained by the expressions of the Donohue method explained in [39].

3.2. Environment Preparation

Taking into account the descriptions and formulas in Section 3.1, the dataset was generated by implementing all of the explained equations in MATLAB. The Equations (1)–(28) were implemented in different function blocks, together with the main code program, which uses the MATLAB function "fzero" to iterate and solve each STHX case. The dataset was obtained in a time of about two hours, using a standard windows laptop (core i7 7th Gen and 16 Gb of RAM).

A MacBook pro i5 computer with 16 GB of RAM was used to develop the NNs. To develop the code, the Python programming language, version 3.9 was used with the numpy, sklearn, keras and matplotlib libraries. Specifically, each of the NNs took an average of 2.5 h to run with 100 epochs.

3.3. Implementation of the NN Model

A NN is a computational model that makes use of different interconnected layers to send information to each other and compute a series of operations [41].

In this particular case, a set of open-source libraries for artificial intelligence were used. Specifically, the libraries selected were the ones provided by tensorflow, sklearn [42].

For this experimentation seven different NNs were implemented. Three of them were mono-objective, one per objective to predict: exchanged heat, pressure drop on shell side and pressure drop on tubes side. Three of the multi-objective NNs aim to predict two targets and the last one predicts the three targets simultaneously. The last multi-objective NN was also used to develop an INN, which is used to find the optimal configuration of the STHX.

To achieve this, the seven initial networks made use of the dataset generated in Section 3.1 to be trained.

The first step, to start developing the NNs, is to preprocess the data to normalise it using the normalisation function minMaxScaler().

Secondly, the NNs were composed of three internal layers, which are explained below in this section. To make these layers learn, activation functions are often used, which are functions added to an artificial NN helping them to learn complex data patterns.

The first layer used the ReLu activation function [31].

$$f(\mathbf{x}) = \max(0, \mathbf{x}). \tag{31}$$

This function enabled better training of the NNs. The second layer used the ReLu activation function as well. While, the third layer was programmed with a linear activation function, which is nothing more complex than a representation of a line in a Cartesian plane.

$$f(\mathbf{x}) = m\mathbf{x} + b. \tag{32}$$

Once the NN was configured, the validation process for each of them was carried out as follows: firstly, the dataset was divided into training and test. Subsequently, each NN performed a total of 100 laps or epochs. This took into account the mean square error (mse) for the NN's validation, as well as the mean absolute error (mae) to recalculate the weights in the activation functions. Lastly, the ADAM algorithm was used to optimise these weights. This serves to lay the foundation for the ultimate NN, the INN.

As indicated above, an INN with backpropagation was proposed and used to solve the inverse heat problem. The proposed method relies on the restrictions of the three different outputs $\mathbf{Y} = \{y_1,\ y_2,\ y_3\}$ (exchanged heat, pressure loss in the tube and pressure loss in the casing) to achieve the optimal initial inputs $\mathbf{X}$ in an intelligent way with high accuracy and minimum loss. To this end, the proposed NN has 12 elements in the input layer ($\mathbf{X} = \{x_i\},\ i = 1,\ \ldots, 12$), that each of these variables have three categories, except one of those that allows 25 distinct levels. As aforementioned, the $\mathbf{Y}$ output layer has three different values: exchanged heat (y_1), pressure loss in the tube (y_2) and pressure loss in the shell (y_3). They considered three hidden layers, in which the ReLu (for the first and the second layers) and the linear (in the last layer) activation functions were applied. Figure 4 shows a block diagram for the proposed tri-objective NN, in which is based the developed INN; the inputs; and outputs of NN as follows:

The performance of the NN was determined based on the mean squared error (MSE) between the NN's actual output and the desired output, besides the corresponding accuracy.

With regard to backpropagation procedure, we firstly found the two closest values to the given desired heat (z) (one of them below z; the other one, above z).

$$z_{\text{below}} = \min\left(\text{dist}\left(z, y_{1_j}\right)\right),\ j = 1\ldots,\ m \text{ and } y_{1_j} <= z \tag{33}$$

$$z_{\text{above}} = \min\left(\text{dist}\left(z, y_{1_j}\right)\right),\ j = 1\ldots,\ m \text{ and } y_{1_j} >= z \tag{34}$$

where m reflects the exchanged heat's dimension.

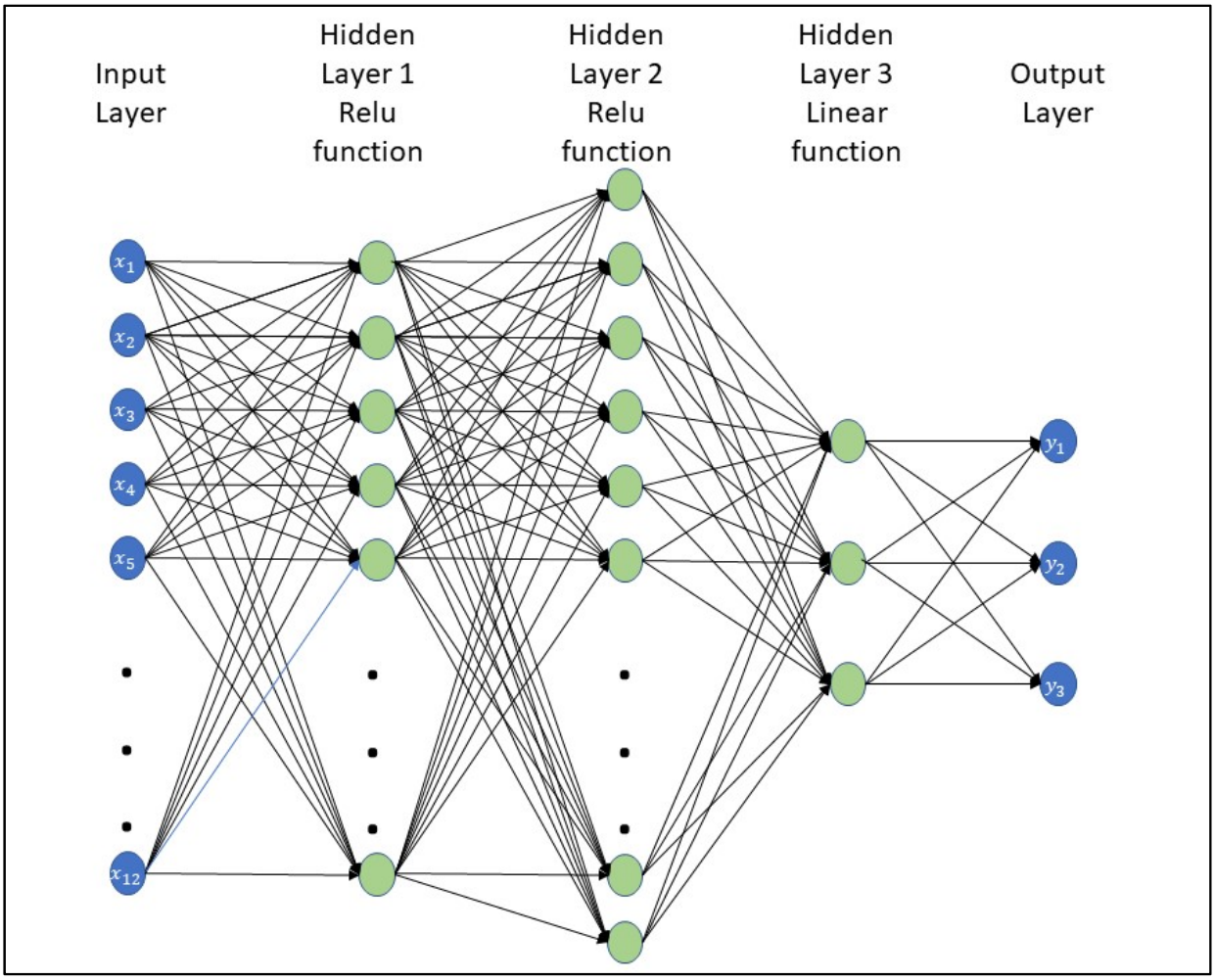

Figure 4. Tri-bjective NN block diagram.

As the next step, we obtained the two configurations ($\mathbf{w}_{\text{below}}$ and $\mathbf{w}_{\text{above}}$) of the input values related to the z_{below} and z_{above} ones. We defined the components of the new $\mathbf{X}' = [x'_i]$ $(i = 1, \ldots, 12)$ as follows:

$$x'_i = \begin{cases} w_{\text{below}i} & \text{if } w_{\text{below}i} = w_{\text{above}i} \\ X[i] & \text{if } w_{\text{below}i} \neq w_{\text{above}i} \end{cases} \tag{35}$$

where $\mathbf{w}_{\text{below}i}$ is a 1×1 matrix and $\mathbf{X}[i]$ is a 1×3 or a 1×25 matrix, upon the variables considered in the input, yielding to the subsequent structure (as an example):

$$\mathbf{X}' = [\, \mathbf{X}[1], \ldots, \mathbf{w}_{\text{below}}[6], \ldots, \mathbf{w}_{\text{below}}[11], \mathbf{X}[12]] \tag{36}$$

To create the synthetic samples from a given $\mathbf{X}'$, all the possible combinations of the $\mathbf{X}'$ components were taken into account. This means that the final number of variants (say $\mathbf{X}''$) would be the $3^n \times 25^m$, where $n =$ number of $\mathbf{X}'[i]$ with three components and $m =$ number of $\mathbf{X}'[i]$ with 25 levels.

Each of the resulting synthetic variations in $\mathbf{X}'$ were considered as new input values of the NN to obtain their corresponding predictions. Those predicted values should require the following conditions to be considered as valid ones:

(a) to be within the 5% interval range of the desired heat exchange.
(b) the loss pressure in the tube and pressure loss in the shell are between 0 and 1.

The synthetic combination $\mathbf{X}'$ that its prediction fulfilled the above-mentioned conditions was selected as the desired final input configuration.

4. NN Model Training and Validation Results

The results obtained are shown in the following Figures 4–10. In each of the figures, two graphs can be seen: the first one (a) shows the loss recorded in each epoch by the NN. As already mentioned, the metric used to measure the loss is the mse. The second one shows the prediction accuracy of the developed NN. Both graphs show the result obtained during the training and validation phases.

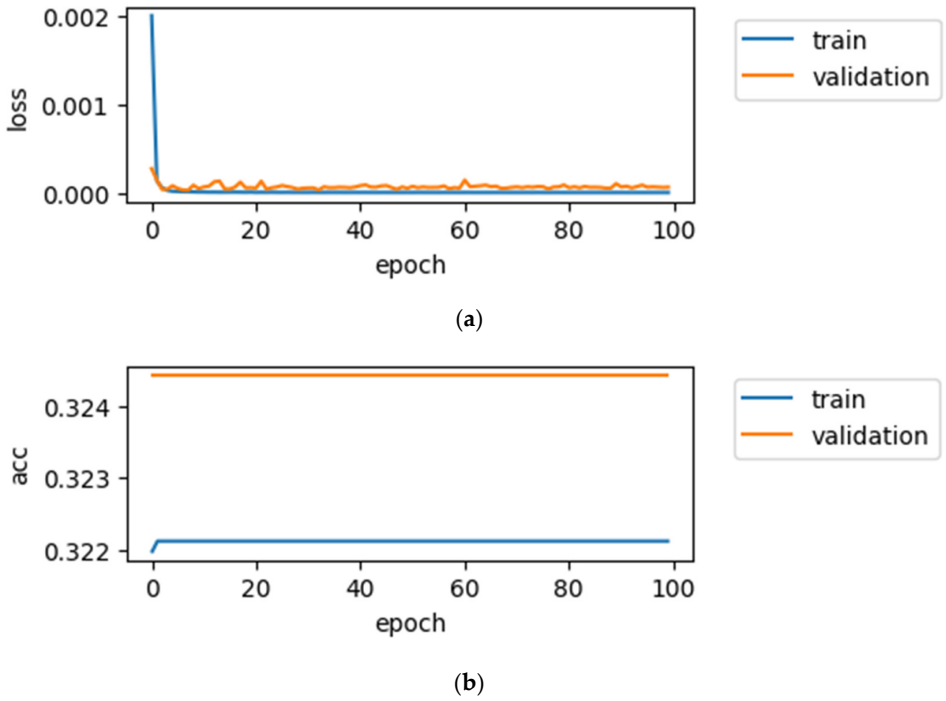

Figure 5. Results for the XH NN. (**a**) Loss metric of the NN. (**b**) Accuracy of predictions.

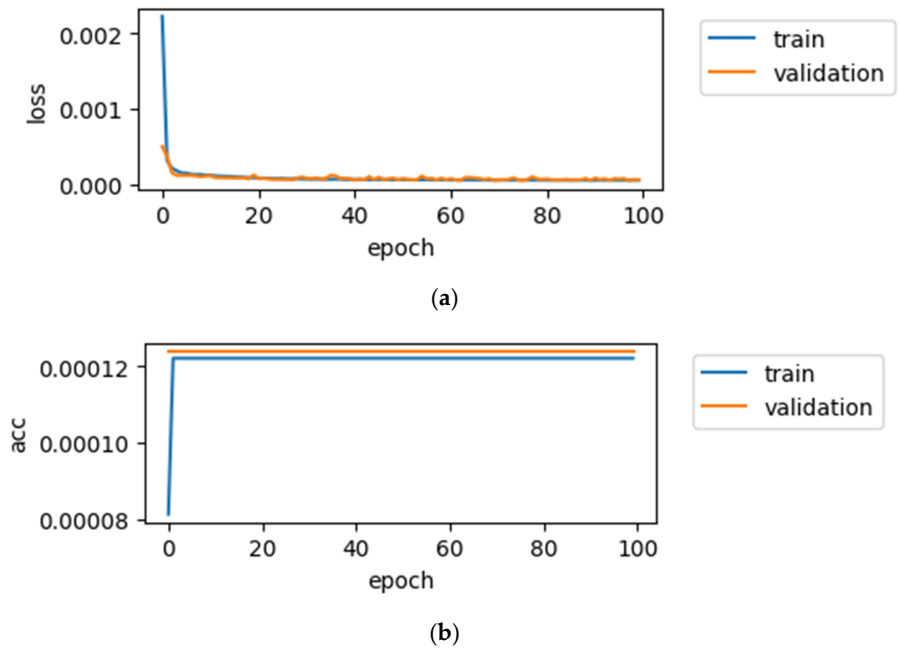

Figure 6. Results for the PDSS NN. (**a**) Loss metric of the NN. (**b**) Accuracy of predictions.

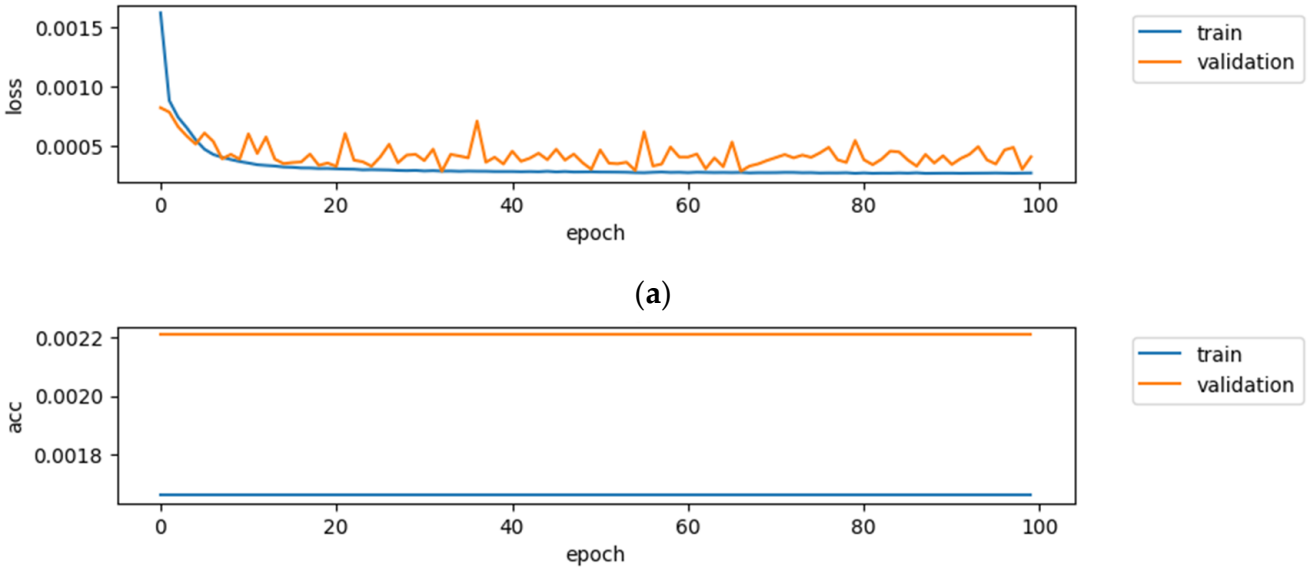

Figure 7. Results for the PDTS NN. (**a**) Loss metric of the NN. (**b**) Accuracy of predictions.

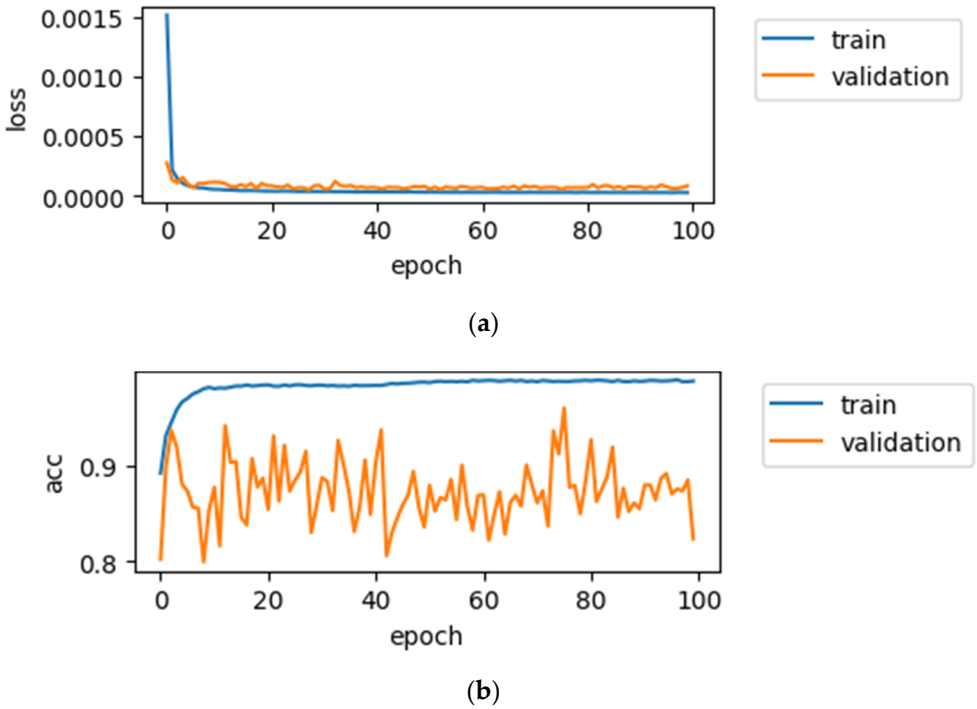

Figure 8. Results for the XH and PDSS NN. (**a**) Loss metric of the NN. (**b**) Accuracy of predictions.

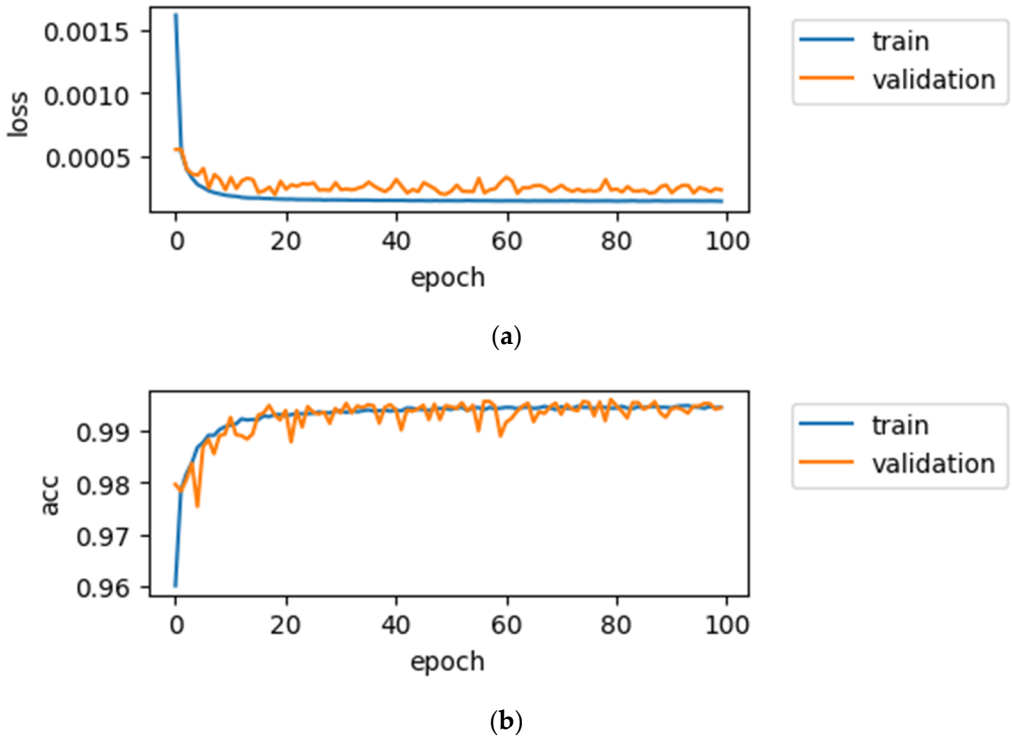

Figure 9. Results for the HX and PDTS NN. (**a**) Loss metric of the NN. (**b**) Accuracy of predictions.

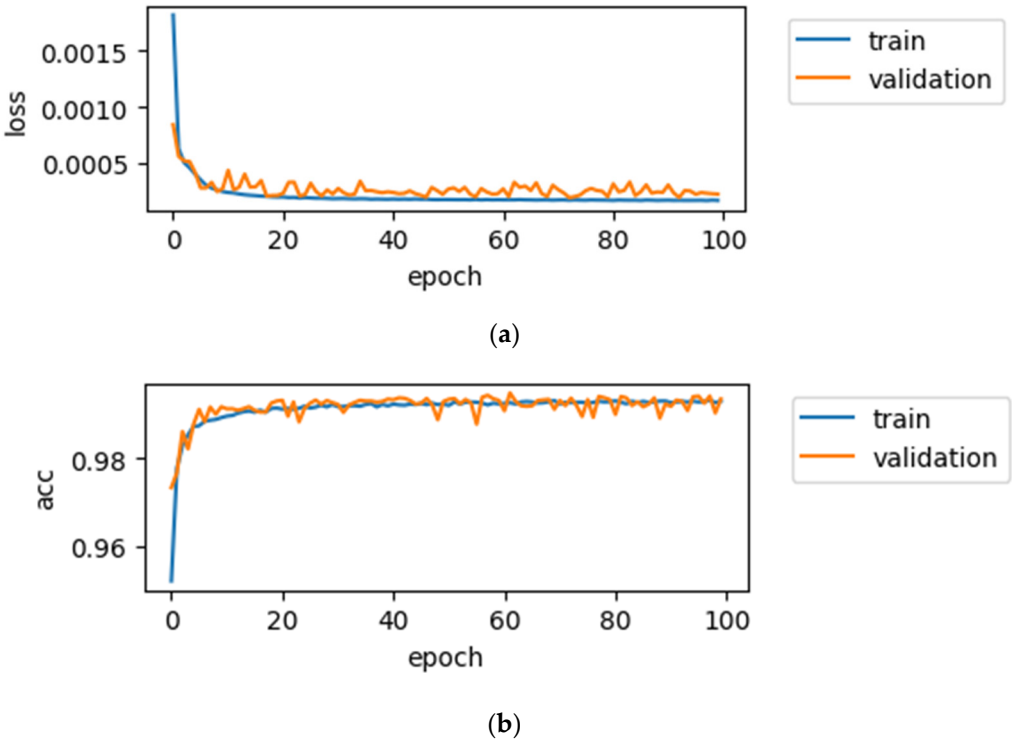

Figure 10. Results for the PDTS and PDSS NN. (**a**) Loss metric of the NN. (**b**) Accuracy of predictions.

4.1. Mono-Objective NNs Results

Figure 5 shows the results for the mono-objective NN of exchanged heat (XH). In the case of the loss (a), values very close to 0 are obtained from the first epochs of the system. It can also be seen that these data are very close to those obtained in the validation phase, although the validation data are slightly higher than those obtained during training. In the second graph (b), it can be seen how the prediction accuracy maintains a stable result since

the first epochs. This mono-objective network generated provides an accuracy of around 32% in both training and validation.

Figure 6 shows the results obtained by the mono-objective NN for pressure drop on the shell side (PDSS). Following the same scheme as in Figure 4, we can see that the results of the training loss (a) are close to 0 from the first epochs, having also a very small slope towards 0 in the rest of the epochs, stabilising around epoch 40. In this case, it is again observed that the results obtained in the validation are more similar to those of the training, than in the case of Figure 4. On the other hand, in the accuracy output (b), it is found that both in the training and in the validation, since the first epochs, the accuracy does not improve, nor does it reach 1%. This shows that it is a poor approximation.

Figure 7 shows the outputs of the NN for the pressure drop in the tubes side (PDTS). In this new case, the loss (a) registers values very close to 0 since the beginning. On the one hand, it can be observed that in the training, the stabilisation of the result, closer to 0, is found from epoch 30 onwards. On the other hand, the validation results do not have a high variability, but they do not reach a stable value in the whole series. In fact, in the last epochs it obtains one of the worst loss values. As for the accuracy (b), a similar scenario to the one in the other two single-target NNs is found again. Stable results, both in training and validation, which do not improve with time and generate a very poor result, which does not reach 1% of correct predictions.

In view of the data provided by these three mono-objective NNs, are presented below the results of the three multi-objective NNs developed that combine in pairs the three mono-objective NNs, already presented.

4.2. Multi-Objective NNs Results

Figure 8 reflects the multi-objective NN results for the combination of the XH and PDSS targets. In loss records graph (a), it is shown that the results are close to 0 from the first epochs, both in training and validation. As it is shown in the Figure 8, both stabilise at the same values. As for accuracy (b), in the case of training, it is observed that in the first epochs it starts with an accuracy of 90%, increasing significantly to about 98% during the first 20, reaching 99% in the last epochs. In contrast, the obtained validation results are not as good as the training ones. It is registered a high variation in all epochs, ranging from 80% to 93%. Only the first epoch obtained an accuracy of almost 100%, which can be assumed to be more due to coincidence than to learning the system itself.

Figure 9 shows the results of the second multi-objective NN, which is targeting the XH and PDTS. The loss metric (a) shows in this case a similar behaviour, in training, to the other NNs with values very close to 0 from the beginning of the epochs. In turn, the performance of the model observed in validation is relatively stable since the beginning. Accuracy (b) starts with values above 95% in training from the very beginning, soon reaching values of almost 99% and remaining stable until the end. In validation it follows the same distribution as in training, with small nonsignificant variations and with values close to 99% during most of the epochs.

Figure 10 shows the results for the last multi-objective NN with two targets, being this time the two pressure losses PDSS and PDTS. As for loss (a), it repeats a similar behaviour to the previous NNs both in training and validation, obtaining values close to 0 from the first epochs. In terms of accuracy (b) the results are very good. Both in training and validation, values of almost 99% of correct predictions are quickly reached.

To finish with the multi-objective NNs and once the results of the two targets NNs were presented, is the time for the three targets multi-objective NN outputs, which can be seen in Figure 10.

Figure 11a shows the NN loss output. The loss results reflect a similar performance as in the previous two targets NNs. Both in training and validation it is found values close to 0 from the first epochs. As for the accuracy (b), a truly good performance was obtained with values close to 99% from the beginning.

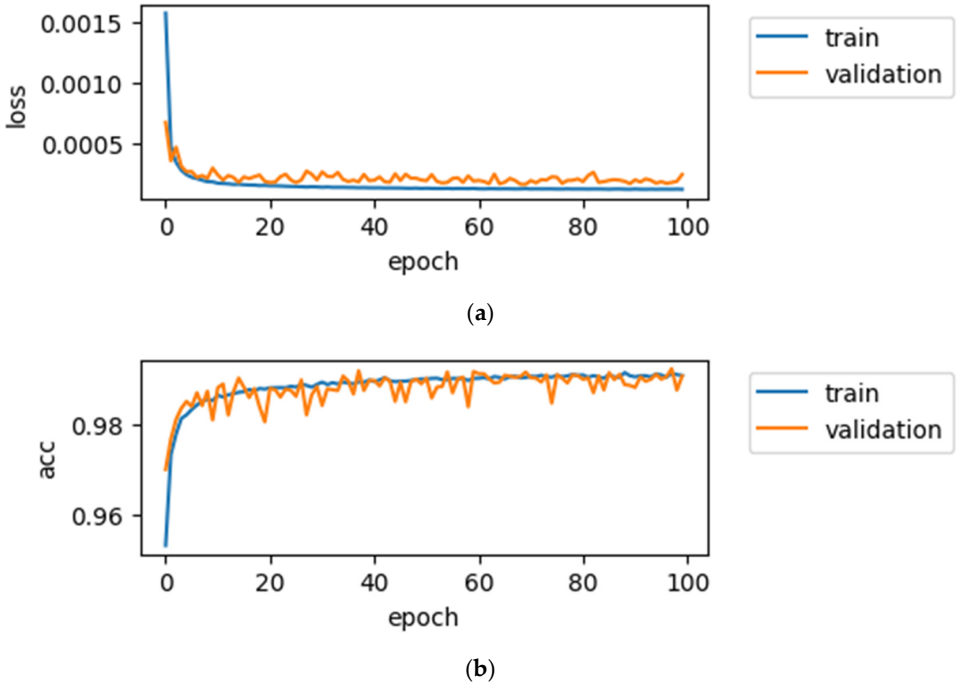

Figure 11. Results for the HX, PDTS and PDSS NN. (**a**) Loss metric of the NN. (**b**) Accuracy of predictions.

5. Problem Formulation and Optimisation Procedure

A multi-objective problem (MOP) can be stated as follows [43,44]

$$\text{minimise/maximise } \mathbf{y} = \mathbf{f}(\mathbf{x}) = (f_1(\mathbf{x}), f_2(\mathbf{x}), \ldots, f_k(\mathbf{x})), \tag{37}$$

$$\text{Subject to the vector of constraints } g(\mathbf{x}) = (g_1(\mathbf{x}), g_2(\mathbf{x}), \ldots, g_m(\mathbf{x}) \leq \mathbf{L}), \tag{38}$$

where $\mathbf{f}: \mathbb{R}^n \to \mathbb{R}^k$ is the objective function, $\mathbf{x} = (x_1, x_2, \ldots, x_n) \in \mathbf{X}$ is the decision vector (or vector of decision variables), and $\mathbf{y} = (y_1, y_2, \ldots, y_k) \in \mathbf{Y}$ is the objective vector. We denote by $\mathbf{X}$ and $\mathbf{Y} = \mathbf{f}(\mathbf{X})$, the decision space and the objective space, respectively.

The optimisation of the generic STHX can be expressed as a MOP. It will always have a main premise of evacuating a reference value of heat exchanged $\dot{Q}_{\text{ref}}$, so the objective regarding heat exchanged will be the minimisation of the absolute difference of $\dot{Q}(\mathbf{x})$ and $\dot{Q}_{\text{ref}}$, among all the valid configurations of STHX the inverse NN offers.

The other two objectives to be minimised will be the pressure drop on the tube side and on the shell side, presented, respectively, in Equations (29) and (30), as lower pressure drops lead to smaller equipment.

Thus, the objectives function of this MOP is:

$$\text{minimise } \mathbf{y} = \mathbf{f}(\mathbf{x}) = \left(\left|\dot{Q}(\mathbf{x}) - \dot{Q}_{\text{ref}}\right|, hL_{\text{shell}}(\mathbf{x}), hL_{\text{tube}}(\mathbf{x})\right). \tag{39}$$

It can be observed that both models depend on the variables shown in Tables 1–3, which may act as constant values (when imposed by the case of the customer), or decision variables and are encoded in the decision vector x. In our problem, the problem is tri-objective ($n = 3$) $\mathbf{f}(\mathbf{x}) = \left(\left|\dot{Q}(\mathbf{x}) - \dot{Q}_{\text{ref}}\right|, hL_{\text{shell}}(\mathbf{x}), hL_{\text{tube}}(\mathbf{x})\right)$ and, as stated, the aim is to offer a STHX that responds to the heat exchange needs of the customer offering the lightest equipment possible (as lower hL_{shell} and hL_{tube} values lead to smaller equipment needs).

The inverse NN can be easily adapted to any restriction imposed to the problem. In this case, it offers solutions limited to a variation between $\dot{Q}(\mathbf{x})$ and $\dot{Q}_{ref}$ of a 5%, it can be stated that the restriction of the problem is the following:

$$g(\mathbf{x}) = \left(\left| \dot{Q}(\mathbf{x}) - \dot{Q}_{\text{ref}} \right| / \dot{Q}_{\text{ref}} \leq 0,05 \right), \tag{40}$$

The optimisation procedure of the case bases on the creation of a Pareto front with all the solutions generated by the inverse NN, discarding the dominated ones. Knowing that a Pareto front is a set of points in parameter space (the space of decision variables) that have noninferior fitness function values, the decision maker automatically receives a set of multi-objective optimal solutions to then select one based on additional criteria.

6. Application Case

One already installed equipment of ARA TT was used as application case. The system is a STHX designed by ARA TT for one of its customers. The values of the already suboptimal configuration of STHX of ARA TT are almost confidential and just the values of $\dot{Q}_{\text{ref}} = 77,653$ kcal/h, $hL_{\text{tube}} = 0.0365$ bar and $hL_{\text{shell}} = 0.4938$ bar can be shown.

Restrictions may not be imposed only to the objective vector, but as well to the values design variables may take. In this case, the customer fixed the number of design variables that should not change its value (the oil mass flow, the oil entry temperature, etc.), allowing ARA TT to offer a more personalised analysis of the problem.

Figure 12 and Table 5 show the Pareto front results obtained in the simulation under the aforementioned conditions.

The set of solutions satisfies the constraints of the problem. As well, most of the solutions are nondominated compared to initial ARA TT's solution. Specifically, all but numbers 12 and 13 are solutions that ARA's one dominates, and we did not include this dominated combination for the optimisation. Thus, decision makers can select among the solutions that fit their preferences taking into account other 'posteriori' restrictions.

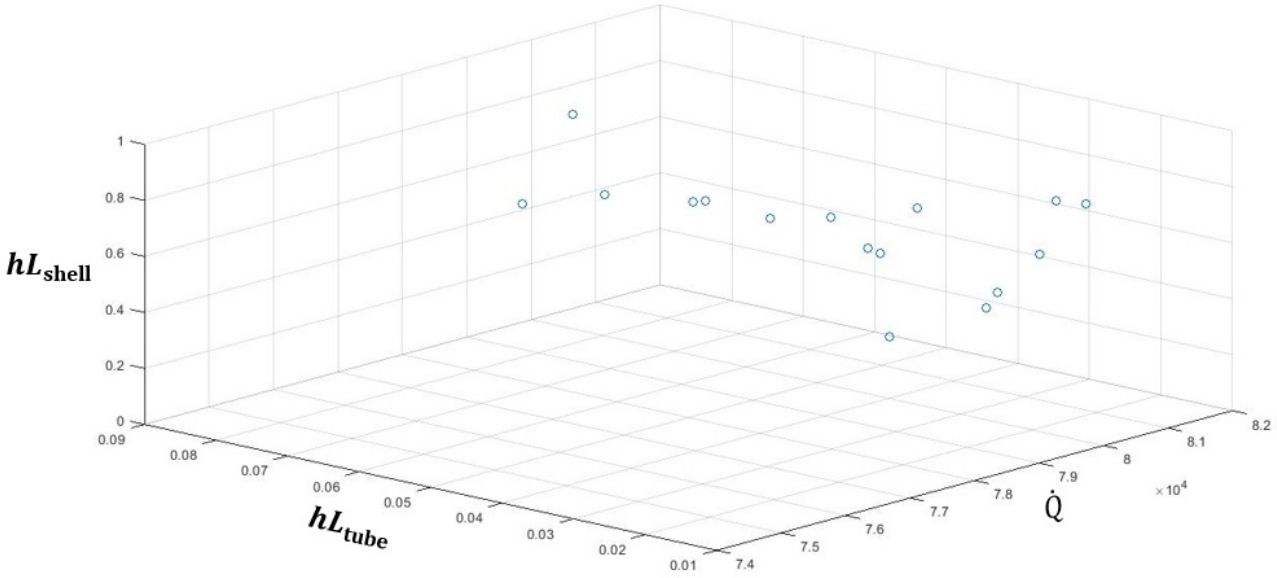

Figure 12. Optimisation results.

Table 5. Optimisation results.

Solution Number	$\dot{Q}$ [kcal/h]	hL_{tube} [bar]	hL_{shell} [bar]
1	81,198.04	0.02737894	0.7027474
2	78,736.02	0.03672727	0.7452056
3	81,197.09	0.03721624	0.26536497
4	80,731.984	0.06314652	0.46797386
5	81,278.98	0.05148795	0.07528893
6	77,753.195	0.02269435	0.7754289
7	80,982.29	0.02783447	0.52240056
8	78,144.21	0.01932829	0.91309184
9	80,042.266	0.01290853	0.8427845
10	81,196.485	0.02474283	0.52855389
11	80,361.836	0.08749065	0.7260448
12	76,647.36	0.03722592	0.9247213
13	76,434.78	0.0476222	0.90788853
14	78,283.484	0.05011504	0.7540955
15	80,860.34	0.04898805	0.41301143
16	81,058.35	0.03442306	0.34464616

7. Discussion

The results obtained demonstrate the validity and usefulness of the developed tool. The NNs developed for this case are capable of precisely predicting the values of the STHX to model, with a level of error that is considered negligible by ARA TT. The inverse NN offers the complete subset of solutions valid for exchanging a predetermined amount of heat. The application of a selection procedure to the INN, such as the Pareto front, allows ARA TT to offer a set of multi-objective optimal solutions so that the designer can select one or another based on additional criteria. Thus, ARA TT can use it as an additional tool for the validation of the designs of STHX they project. For this reason, this approach can be considered as a practical and realistic way to improve the traditional industrial design of the STHX method, reducing the number of potential errors to occur.

As indicated in the literature review, optimisation of STHX is a topic that is gaining more importance in recent years, while their multi-objective optimisation is calling the attention of researchers in recent months. After the literature review, we concluded that classical solutions that are not based exclusively on NNs cannot be left at companies as stand-alone tools, because changes in the models of STHX, in their restrictions or even in the objective functions would need intense reprograming. Neither the RELU algorithm used in the NNs nor an INN have been ever used for this STHX optimisation case. Thus, both the complete applicability of the developed solution and the novelty of the type of algorithm implemented can be defined as the innovative factors of this paper.

The main limitation of this research is the potential incompatibility, since this initiative does not work for every type of heat exchanger. It is useful to model STHX between the parameters studied in the dataset, but not for other cases. Evidently, this fact opens a path for future works: this method could always continue improving the results and extending its limits, while adding more cases to the dataset. This means that it could be always a much more effective solution for the design problem. Nevertheless, it has a limitation itself, because the more cases the dataset has, the more execution time the NN will need.

For the moment, the developed tool may have room for improvement regarding cost of training (of the NN), but not in terms of simplicity and easiness to maintain. Evidently, further investigation will be oriented to obtain tools that are jointly easy to maintain and train.

8. Conclusions

This work presents the design of a multi-objective sizing tool for STHX. It was developed under a university-industry collaboration framework. The convenience of NN is increasing day by day and this paper is another good proof of the fact. The design of STHX

optimisation tools using artificial intelligence algorithms is a visited topic in the literature, nevertheless, the degree of actual implementations in companies has not been documented until this presented work. The entire procedure is validated by ARA TT, the company taking part in the project. The developed method was implemented using a simulated dataset contrasted with the organisation.

This work aimed to demonstrate the feasibility of implementing artificial intelligence tools in the design of heat exchangers in industry. This aim was proven to be accomplished since the developed tool satisfied every ARA TT's industrial requirements.

The simulated dataset was modeled using MATLAB to develop a theoretical STHX calculator. This dataset was used to train three mono-objective NNs, one per objective to be optimised. Once trained, the three were used to train the four multi-objective NNs. Three of them had two targets and the fourth one targeted the three main outputs (XH, PDSS, PDTS). The seven NNs were successfully developed, as presented in results section. The last NN with three targets had reached an accuracy of 99% which is an incredible result for these types of cases.

The three target multi-objective NN was used to develop an inverse NN as well. This inverse NN made it possible to set up the optimum STHX, as can be seen in the application case section. In this specific case two design parameters, pressure drop and heat transfer rate, were jointly optimised. Thus, this article also proved that this tool could help companies like ARA TT to improve their business activity.

Introducing cost optimisation directly to the NN model is a possible future research line. It is shown that NN can help in the present and with this future guideline will help to improve the ARA's industrial business performance. It is also worth remarking that other partners of the Deusto Digital Industry Chair have shown their interest in this initiative. Therefore, the efforts of the chair will be oriented to consolidate this approach.

Author Contributions: J.L.d.A.H. and U.A.-L. writing and investigation; J.G.d.l.P. and F.C., conceptualisation, writing and investigation; A.G., project administration, investigation, writing and supervision and J.R., funding acquisition. All authors have read and agreed to the published version of the manuscript.

Funding: Accenture: Inzu Group, Lantek, Fundación Telefónica and BBK fundazioa.

Institutional Review Board Statement: Not applicable.

Informed Consent Statement: Not applicable.

Data Availability Statement: Data available on request to restrictions eg privacy or ethical.

Acknowledgments: We would like to thank the partner of the Deusto Digital Industry Chair, as well as ARA TT, for the interest and support shown during this research.

Conflicts of Interest: The authors declare no conflict of interest.

References

1. Webb, R.L. Enhanced Heat Transfer. *Am. Soc. Mech. Eng. Heat Transf. Div. HTD* **1992**, *202*, 301–312.
2. Koukou, M.K.; Dogkas, G.; Vrachopoulos, M.G.; Konstantaras, J.; Pagkalos, C.; Lymperis, K.; Stathopoulos, V.; Evangelakis, G.; Prouskas, C.; Coelho, L.; et al. Performance evaluation of a small-scale latent heat thermal energy storage unit for heating applications based on a nanocomposite organic PCM. *ChemEngineering* **2019**, *3*, 88. [CrossRef]
3. Agnew, B.; Tam, I.C.K.; Shi, X. Optimization of heat and mass exchange. *Processes* **2020**, *8*, 314. [CrossRef]
4. Shah, R.K.; Sekuli, D.P. *Fundamentals of Heat Exchanger Design*; John Wiley & Sons, Inc.: Hoboken, NJ, USA, 2003; ISBN 0471321710.
5. Rao, R.V.; Saroj, A. Multi-objective design optimization of heat exchangers using elitist-Jaya algorithm. *Energy Syst.* **2018**, *9*, 305–341. [CrossRef]
6. Kakaç, S.; Liu, H.; Pramuanjaroenkij, A. *Heat Exchangers: Selection, Rating, and Thermal Design*, 4th ed.; CRC Press of Taylor & Francis Group: Boca Raton, FL, USA, 2020; ISBN 9781138601864.
7. Valencia, G.; Núñez, J.; Duarte, J. Multiobjective optimization of a plate heat exchanger in a waste heat recovery organic rankine cycle system for natural gas engines. *Entropy* **2019**, *21*, 655. [CrossRef]
8. Renedo Estébanez, C.J.; Ortiz Fernandez, A.; Perez Remesal, S.F.; Fernandez Diego, I.; Mañana Canteli, M.; Fernandez Fernandez, M. Cogeneracion Mediante Recuperacion Energetica De Calor De Gases De Escape. *Dyna Ing. E Ind.* **2011**, *86*, 105–117. [CrossRef]

9. Fernández Diaz, P. XV-Intercambiadores de Calor Método de la (LMTD). In *Intercambiadores de Calor*; Biblioteca Sobre Ingeniería energética: Santander, Spain; pp. 269–286.
10. Dezfoli, A.R.A.; Mehrabian, M.A.; Saffaripour, M.H. Two dimensional temperature distributions in plate heat exchangers: An analytical approach. *Mathematics* **2015**, *3*, 1255–1273. [CrossRef]
11. Sarafraz, M.M.; Safaei, M.R.; Tian, Z.; Goodarzi, M. Thermal Assessment of Nano-Particulate Graphene-Water/Ethylene Glycol (WEG 60:40) Nano-Suspension in a Compact Heat Exchanger. *Energies* **2019**, *12*, 1219. [CrossRef]
12. Lazova, M.; Huisseune, H.; Kaya, A.; Lecompte, S.; Kosmadakis, G.; De Paepe, M. Performance evaluation of a helical coil heat exchanger working under supercritical conditions in a solar organic rankine cycle installation. *Energies* **2016**, *9*, 432. [CrossRef]
13. Yang, J.; Ma, L.; Bock, J.; Jacobi, A.M.; Liu, W. A comparison of four numerical modeling approaches for enhanced shell-and-tube heat exchangers with experimental validation. *Appl. Therm. Eng.* **2014**, *65*, 369–383. [CrossRef]
14. Sahoo, P.K.; Ansari, M.I.A.; Datta, A.K. A computer based iterative solution for accurate estimation of heat transfer coefficients in a helical tube heat exchanger. *J. Food Eng.* **2003**, *58*, 211–214. [CrossRef]
15. Sun, Y.; Wang, X.; Long, R.; Yuan, F.; Yang, K. Numerical investigation and optimization on shell side performance of a shell and tube heat exchanger with inclined trefoil-hole baffles. *Energies* **2019**, *12*, 4138. [CrossRef]
16. Tran, H.K.; Son, H.H.; Van Duc, P.; Trang, T.T.; Nguyen, H.N. Improved genetic algorithm tuning controller design for autonomous hovercraft. *Processes* **2020**, *8*, 66. [CrossRef]
17. Stajkowski, S.; Kumar, D.; Samui, P.; Bonakdari, H.; Gharabaghi, B. Genetic-algorithm-optimized sequential model for water temperature prediction. *Sustainability* **2020**, *12*, 5374. [CrossRef]
18. Freitas, D.; Lopes, L.G.; Morgado-Dias, F. Particle Swarm Optimization: A historical review up to the current developments. *Entropy* **2020**, *22*, 362. [CrossRef]
19. Su, P.; Cai, C.; Song, Y.; Ma, J.; Tan, Q. A hybrid diffractive optical element design algorithm combining particle swarm optimization and a simulated annealing algorithm. *Appl. Sci.* **2020**, *10*, 5485. [CrossRef]
20. Tan, C.K.; Ward, J.; Wilcox, S.J.; Payne, R. Artificial neural network modelling of the thermal performance of a compact heat exchanger. *Appl. Therm. Eng.* **2009**, *29*, 3609–3617. [CrossRef]
21. Wen, J.; Gu, X.; Wang, M.; Wang, S.; Tu, J. Numerical investigation on the multi-objective optimization of a shell-and-tube heat exchanger with helical baffles. *Int. Commun. Heat Mass Transf.* **2017**, *89*, 91–97. [CrossRef]
22. Wang, X.; Zheng, N.; Liu, Z.; Liu, W. Numerical analysis and optimization study on shell-side performances of a shell and tube heat exchanger with staggered baffles. *Int. J. Heat Mass Transf.* **2018**, *124*, 247–259. [CrossRef]
23. Sadeghzadeh, H.; Aliehyaei, M.; Rosen, M.A. Optimization of a finned shell and tube heat exchanger using a multi-objective optimization genetic algorithm. *Sustainability* **2015**, *7*, 11679–11695. [CrossRef]
24. Tang, S.Z.; Li, M.J.; Wang, F.L.; He, Y.L.; Tao, W.Q. Fouling potential prediction and multi-objective optimization of a flue gas heat exchanger using neural networks and genetic algorithms. *Int. J. Heat Mass Transf.* **2020**, *152*, 119488. [CrossRef]
25. Hojjat, M. Nanofluids as coolant in a shell and tube heat exchanger: ANN modeling and multi-objective optimization. *Appl. Math. Comput.* **2020**, *365*, 124710. [CrossRef]
26. Martin, H. Economic Optimization of Compact Heat Exchangers. In Proceedings of the EF-Conference on Compact Heat Exchangers and Enhancement Technology for the Process Industries, Banff, AB, Canada, 18–23 July 1999.
27. Yang, J.; Oh, S.R.; Liu, W. Optimization of shell-and-tube heat exchangers using a general design approach motivated by constructal theory. *Int. J. Heat Mass Transf.* **2014**, *77*, 1144–1154. [CrossRef]
28. Zheng, N.; Liu, P.; Wang, X.; Shan, F.; Liu, Z.; Liu, W. Numerical simulation and optimization of heat transfer enhancement in a heat exchanger tube fitted with vortex rod inserts. *Appl. Therm. Eng.* **2017**, *123*, 471–484. [CrossRef]
29. Alberdi, E.; Urrutia, L.; Goti, A.; Oyarbide-Zubillaga, A. Modeling the municipalwaste collection using genetic algorithms. *Processes* **2020**, *8*, 513. [CrossRef]
30. Bhargava, S. A Note on Evolutionary Algorithms and Its Applications. *Adults Learn. Math. Int. J.* **2013**, *8*, 31–45.
31. Agarap, A.F.M. Deep Learning using Rectified Linear Units (ReLU). *arXiv* **2018**, arXiv:1803.08375v2.
32. Chai, T.; Draxler, R.R. Root mean square error (RMSE) or mean absolute error (MAE)? -Arguments against avoiding RMSE in the literature. *Geosci. Model Dev.* **2014**, *7*, 1247–1250. [CrossRef]
33. Hara, K.; Saito, D.; Shouno, H. Analysis of function of rectified linear unit used in deep learning. In Proceedings of the International Joint Conference on Neural Networks (IJCNN) 2015, Killarney, Ireland, 12–17 July 2015. [CrossRef]
34. ARA TT. Diseño, Fabricación y Reparación de Intercambiadores de Calor y Recipientes a Presión, así Como Otros Equipos Electro-mecánicos. Available online: https://www.aratt.es/ (accessed on 8 February 2021).
35. ARA TT. *Internal Report—Oil Properties*; ARA TT: Bilbao, Spain, 2019.
36. Salazar Valdez, J.F. Diseño de equipos de transferencia de calor. Ph.D. Thesis, Universidad Autónoma de Nuevo León, San Nicolás de los Garza, Mexico, 2001.
37. Ouardi, E.; Darfi, S.; Khallouq, K.; Mousaid, A. A novel approach for thermal designing a single pass counter flow shell and tube heat exchanger. *Int. J. Mech. Prod. Eng. Res. Dev.* **2020**, *10*, 269–280. [CrossRef]
38. Ravagnani, M.A.; Silva, A.P.; Caballero, J.A. Optimal Shell and Tube Heat Exchangers Design. *Heat Anal. Thermodyn. Eff.* **2011**. [CrossRef]
39. Urquiola, F.M. *Equipos de Intercambio de Calor*, 1st ed.; CADEM (GRUPO EVE): Bilbao, Spain, 1994; ISBN 84-8129-024-6.
40. Mott, R.L. *Mecánica de Fluidos*, 6th ed.; PEARSON Educación: Mexico City, Mexico, 2006; ISBN 0131146807.

41. Mitchel, T.M. Artificial neural networks. *Mach. Learn.* **1997**, *45*, 81–127.
42. Abadi, M.; Barham, P.; Chen, J.; Chen, Z.; Davis, A.; Dean, J.; Devin, M.; Ghemawat, S.; Irving, G.; Isard, M.; et al. TensorFlow: A System for Large-Scale Machine Learning. In Proceedings of the 12th USENIX Symposium on Operating Systems Design and Implementation (OSDI '16), Savannah, GA, USA, 2–4 November 2016; pp. 265–283. [CrossRef]
43. Oyarbide-Zubillaga, A.; Goti, A.; Sanchez, A. Preventive maintenance optimization of multi-equipment manufacturing systems by combining discrete event simulation and multi-objective evolutionary algorithms. *Prod. Plan. Control.* **2008**, *19*, 342–355. [CrossRef]
44. Goti, A.; Oyarbide-Zubillaga, A.; Alberdi, E.; Sanchez, A.; Garcia-Bringas, P. Optimal Maintenance Thresholds to Perform Preventive Actions by Using Multi-Objective Evolutionary Algorithms. *Appl. Sci.* **2019**, *9*, 3068. [CrossRef]